Contribution from the Chemical Thermodynamics Laboratory, Faculty of Science, Osaka University, Toyonaka, Osaka 560, Japan, Department of Chemistry, D-006, University of California at San Diego, La Jolla, California 92093, and School of Chemical Sciences, University of Illinois, Urbana, Illinois 61801

Heat Capacity and Phase Transition of the Mixed-Valence Compound [Fe3O(O2CCH3)6(py)3](CHCl3)[†]

Yuki Kaneko,[1] Motohiro Nakano,[1] Michio Sorai,*,[1] Ho G. Jang,[2a] and David N. Hendrickson*,[2a,b]

Received June 17, 1988

The heat capacity of the mixed-valence complex [Fe3O(O2CCH3)6(py)3](CHCl3), where py is pyridine, has been measured with an adiabatic calorimeter between 14 and 300 K. A phase transition with two peaks closely centered at 207.14 and 208.19 K has been found. The enthalpy and entropy of the phase transition are $\Delta H = 5107 \pm 44$ J mol^{-1} and $\Delta S = 28.10 \pm 0.44$ J K^{-1} mol^{-1}. By comparing the present calorimetric results with available ^{57}Fe Mössbauer, X-ray structural, and solid-state ^{2}H NMR data for the complex with a CDCl$_3$ solvate molecule, we concluded that the phase transition is associated with the onset of intramolecular electron transfer in the mixed-valence Fe3O complexes and the onset of orientational disordering of the chloroform solvate molecules. The former contribution to ΔS is $R \ln 4$ while the latter is $R \ln 8$, where R is the gas constant. The total entropy gain, $R \ln 32$ (=28.82 J K^{-1} mol^{-1}), agrees well with the observed ΔS. In the high-temperature phase, each Fe3O complex is dynamically interconverting between four vibronic states, in one of which the complex has C_3 symmetry and is electronically delocalized. In each of the other three states, the "extra" electron is trapped on one of the iron ions. The contribution for the solvate molecule is in keeping with a model derived from the ^{2}H NMR studies. In this model the C–H vector of the CHCl$_3$ solvate molecule is moving between four equally probable positions, one with the C–H vector along the C_3-symmetry axis, which is also the axis along which the Fe3O complexes are stacked. The other three positions have the C–H vector directed off the C_3 axis on a cone that makes an angle of 24.7° with the C_3 axis. Since the CHCl$_3$ solvate molecule sits on a 32 symmetry site, the number of the total positions of the C–H vector is 8 (4 up and 4 down), and hence the entropy gain for the CHCl$_3$ going from static in one position to moving dynamically between these eight positions is $R \ln 8$. The present complex confirms that dynamics of a solvate molecule in a solid-state lattice dramatically affect the rate of intramolecular electron transfer in mixed-valence complexes. The relationship between the rate of intramolecular electron transfer and disordering of the solvate molecules is discussed by comparing the present results with the phase transitions found in the analogous complexes [Fe3O(O2CCH3)6(4-Me-py)3](CHCl3) and [Fe3O-(O2CCH3)6(4-Me-py)3](CH3CCl3), where 4-Me-py is 4-methylpyridine.

Introduction

Oxo-centered, trinuclear metal acetate complexes with the formula [M^{III}$_2$M^{II}O(O2CCH3)6L3]S form a well-studied category of mixed-valence compounds, where M is a transition-metal element such as iron or manganese, L is a monodentate ligand such as pyridine, monosubstituted pyridine, or water, and S is a solvate molecule that is not explicitly coordinated to the central metal ions but is stoichiometrically amalgamated in the crystal lattice. It has been shown recently that dynamics in a solid-state lattice affect dramatically the rate of intramolecular electron transfer in a number of these mixed-valence compounds.[3–11] The onset of motion of the ligand L[3,10] or solvate S[9,10] has been found to affect the rate of electron transfer. For instance, the rate of intramolecular electron transfer in the mixed-valence compound with a composition [Fe3O(O2CCH3)6(py)3](py), where py is pyridine, exceeds the Mössbauer time scale ($\sim 10^8$ s^{-1}) as the temperature is increased above ~ 190 K, while the nonsolvated analogue, [Fe3O(O2CCH3)6(py)3], remains in a valence-trapped state from 4.2 up to 315 K.[3,5]

Interestingly, the electron localization–delocalization of mixed-valence Fe3O complexes has been shown to involve phase transitions.[3–6,9] Microscopic and/or dynamic aspects occurring in these phase transitions have been probed by single-crystal X-ray diffraction studies as well as a number of spectroscopic techniques such as ^{57}Fe Mössbauer, solid-state ^{2}H NMR, EPR, IR, and Raman spectroscopies. However, these spectroscopic methods have intrinsic "selection rule" and "time scale" characteristics. In contrast, heat capacity measurements can serve as a useful tool to elucidate the macroscopic aspects of these phase transitions. In particular, the knowledge of the entropy gain at a phase transition is indispensable to an interpretation of how many molecular freedoms are gained in a phase transition. For a thorough understanding of these phase transitions, therefore, the complementary role of the microscopic and calorimetric methods is fundamentally important. Successful interplay between them has been demonstrated for a couple of mixed-valence compounds.[4,6,11,12]

The title compound, hexakis(μ-acetato)(μ_3-oxo)tris(pyridine)iron(II)diiron(III)—chloroform, [Fe3O(O2CCH3)6(py)3]-(CHCl3), crystallizes in the rhombohedral space group $R32$[13] at 298 K, as does [Fe3O(O2CCH3)6(py)3](py).[7] Planar Fe3O cores and disordered chloroform solvate molecules are stacked in alternate sites of 32 symmetry along the 3-fold (i.e., c) axis. As reproduced in Figure 1,[13] the ^{57}Fe Mössbauer spectrum for this compound below ~ 150 K shows two quadrupole-split doublets of area ratio 2:1 (Fe^{III}:Fe^{II}). As the sample temperature is increased, a third doublet appears at the expense of the initial two doublets, and finally above ~ 210 K a single average-valence doublet remains.[13] One can, therefore, expect a phase transition around 200 K.

It is of great interest that both of the solvate molecules, planar pyridine and trigonal-pyramidal chloroform, sit on the C_3 axis in [Fe3O(O2CCH3)6(py)3]S and satisfy the 32 symmetry in their valence-detrapped phases. In the case of the pyridine solvate complex, the pyridine solvate molecules are disordered about two axes parallel and perpendicular to the molecular axis of the

(1) Osaka University.
(2) (a) University of Illinois. (b) University of California at San Diego. Request reprints at this address.
(3) Oh, S. M.; Hendrickson, D. N.; Hassett, K. L.; Davis, R. E. *J. Am. Chem. Soc.* **1984**, *106*, 7984.
(4) Oh, S. M.; Kambara, T.; Hendrickson, D. N.; Sorai, M.; Kaji, K.; Woehler, S. E.; Wittebort, R. J. *J. Am. Chem. Soc.* **1985**, *107*, 5540.
(5) Oh, S. M.; Hendrickson, D. N.; Hassett, K. L.; Davis, R. E. *J. Am. Chem. Soc.* **1985**, *107*, 8009.
(6) Sorai, M.; Kaji, K.; Hendrickson, D. N.; Oh, S. M. *J. Am. Chem. Soc.* **1986**, *108*, 702.
(7) Woehler, S. E.; Wittebort, R. J.; Oh, S. M.; Hendrickson, D. N.; Inniss, D.; Strouse, C. E. *J. Am. Chem. Soc.* **1986**, *108*, 2938.
(8) Kambara, T.; Hendrickson, D. N.; Sorai, M.; Oh, S. M. *J. Chem. Phys.* **1986**, *85*, 2895.
(9) Woehler, S. E.; Wittebort, R. J.; Oh, S. M.; Kambara, T.; Hendrickson, D. N.; Inniss, D.; Strouse, C. E. *J. Am. Chem. Soc.* **1987**, *109*, 1063.
(10) Oh, S. M.; Wilson, S. R.; Hendrickson, D. N.; Woehler, S. E.; Wittebort, R. J.; Inniss, D.; Strouse, C. E. *J. Am. Chem. Soc.* **1987**, *109*, 1073.
(11) Sorai, M.; Shiomi, Y.; Hendrickson, D. N.; Oh, S. M.; Kambara, T. *Inorg. Chem.* **1987**, *26*, 223.
(12) Sorai, M.; Nishimori, A.; Hendrickson, D. N.; Dong, T. Y.; Cohn, M. J. *J. Am. Chem. Soc.* **1987**, *109*, 4266.
(13) X-ray analysis and ^{2}H NMR and ^{57}Fe Mössbauer spectroscopy of [Fe3O(O2CCH3)6(py)3](CHCl3): Jang, H. G.; Geib, S. J.; Kaneko, Y.; Nakano, M.; Sorai, M.; Rheingold, A. L.; Montez, B.; Hendrickson, D. N. *J. Am. Chem. Soc.* **1989**, *111*, 173.
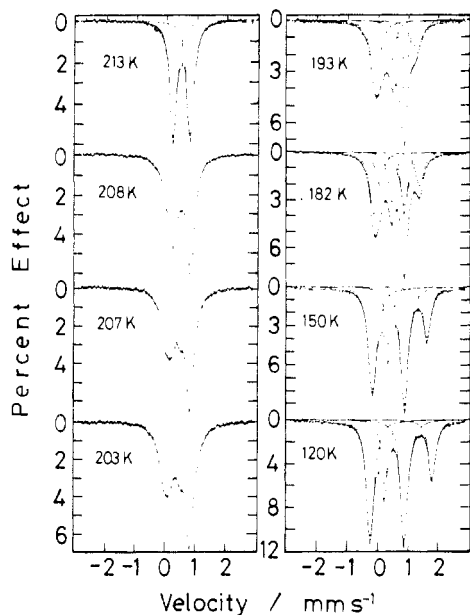
Figure 1. Variable-temperature ^{57}Fe Mössbauer spectra of [Fe$_3$O-(O$_2$CCH$_3$)$_6$(py)$_3$](CHCl$_3$). Several spectra were least-squares fit to Lorentzian line shapes.

Figure 2. Heating DTA runs for (a) [Fe$_3$O(O$_2$CCH$_3$)$_6$(py)$_3$](CHCl$_3$), (b) [Fe$_3$O(O$_2$CCH$_3$)$_6$(4-Me-py)$_3$](CHCl$_3$), and (c) [Fe$_3$O(O$_2$CCH$_3$)$_6$-(4-Me-py)$_3$](CH$_3$CCl$_3$). The numbers indicate temperatures in K.

pyridine solvate molecule.[9] In contrast to this, in the case of the chloroform solvate complex, the situation seems to be simple because the chloroform molecule itself has a C_3 axis. Hence the 32 symmetry is fulfilled when a CHCl$_3$ molecule is disordered equally in two positions, one with the C–H vector pointing up along the C_3 axis and the other with the C–H vector pointing down along the C_3 axis. One of the objectives of the present paper was to elucidate, on the basis of heat-capacity measurements, whether the chloroform solvate molecules are coupled with the intramolecular electron transfer in the central Fe$_3$O core through such a simple disordering process or through a more complicated process.

The classical structure for the trinuclear mixed-valence complexes consists of the central Fe$_3$O core in which two of the iron ions are assigned as Fe^{III} and the third as Fe^{II}. The "extra" d electron is localized on a single iron ion, and hence the Fe$_3$O core must Jahn–Teller distort into an isosceles triangle. A possible mechanism of the phase transition could involve the onset of fast electron transfer among three iron ions where each Fe$_3$O core structure is changed from a static distortion to a dynamic distortion. In this case, the entropy change due to the intramolecular electron transfer gained in the phase transition should be R ln 3, where R is the gas constant.

Available theories,[14–17] however, have predicted the existence of a nonclassical alternative in the adiabatic potential: the "extra" electron can be coherently delocalized among the three iron ions without any distortion from the equilateral triangle structure. If this kind of static delocalization is thermally accessible together with three dynamical distortions in the electron-delocalized high-temperature phase, the entropy change involved in the phase transition would be R ln 4.

Experimental Section

Sample Preparation. Samples of [Fe$_3$O(O$_2$CCH$_3$)$_6$(py)$_3$](py) were prepared as reported previously.[9] Samples of the chloroform solvate [Fe$_3$O(O$_2$CCH$_3$)$_6$(py)$_3$](CHCl$_3$) were prepared by dissolving the pyridine solvate in CHCl$_3$ under an Ar atmosphere and then slowly evaporating the solution. The heat capacity sample was prepared in three batches of ~7, ~5, and ~4 g. A typical chemical analysis follows. Anal. Calcd for C$_{28}$Cl$_3$Fe$_3$H$_{34}$N$_3$O$_{13}$: C, 37.60; Cl, 11.89; Fe, 18.73; H, 3.83; N, 4.71.
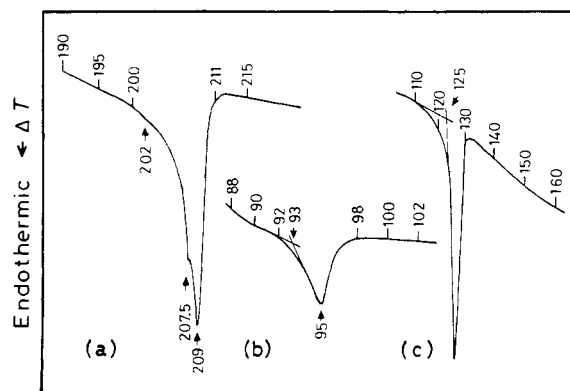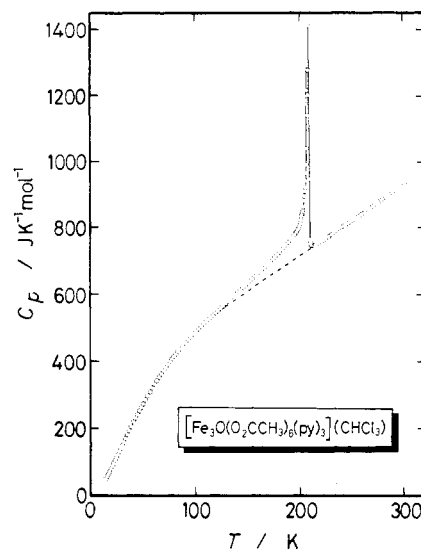
Figure 3. Molar heat capacity of [Fe$_3$O(O$_2$CCH$_3$)$_6$(py)$_3$](CHCl$_3$). Broken curve indicates the normal heat capacity.

Found: C, 37.61; Cl, 12.00; Fe, 18.58; H, 3.85; N, 4.98.

Differential Thermal Analysis (DTA). Preliminary observation of the thermal properties was made with a home-built DTA apparatus that operates between 60 and 530 K.

Heat Capacity Measurements. Heat capacities were measured with an adiabatic calorimeter[18] from 14 to 300 K. A calorimeter cell[19] made of gold-plated copper was loaded with 15.6245 g (or 0.017 467 50 mol) of polycrystalline [Fe$_3$O(O$_2$CCH$_3$)$_6$(py)$_3$](CHCl$_3$) with buoyancy correction assuming a density of 1.34 g cm^{-3}. A small amount of helium gas was sealed in the cell to aid the heat transfer.

Infrared Absorption Spectra. Variable-temperature IR spectra were recorded for Nujol mulls between 96 and 299 K with an infrared spectrophotometer, Model DS-402G (Japan Spectroscopic Co., Ltd.), in the range 4000–400 cm^{-1} and with a far-infrared spectrophotometer, Model FIS-3 (Hitachi, Ltd.), in the range 400–30 cm^{-1}.

Results

As shown in Figure 2a, a heating DTA thermogram for [Fe$_3$O(O$_2$CCH$_3$)$_6$(py)$_3$](CHCl$_3$) exhibits three thermal anomalies. Two of them are large peaks closely centered at 207.5 and 209 K while the third is a tiny anomaly around 202 K. The presence of the two dominant peaks indicates that a phase transition exists in this complex. Although the undercooling phenomenon was not observed for the cooling DTA run within experimental error, the specimen in the adiabatic calorimeter was cooled quite slowly, especially when its temperature passed through the phase-transition region.

(14) Borshch, S. A.; Kotov, I. N.; Bersuker, I. B. *Chem. Phys. Lett.* **1982**, *89*, 381.
(15) Launay, J. P.; Babonneau, F. *Chem. Phys.* **1982**, *67*, 295.
(16) Cannon, R. D.; Montri, L.; Brown, D. B.; Marshall, K. M.; Elliott, C. M. *J. Am. Chem. Soc.* **1984**, *106*, 2591.
(17) Stratt, R. M.; Adachi, S. H. *J. Chem. Phys.* **1987**, *86*, 7156.

(18) Construction of an adiabatic calorimeter workable between 12 and 530 K: Sorai, M.; Kaji, K. Unpublished results.
(19) Ogasahara, K.; Sorai, M.; Suga, H. *Mol. Cryst. Liq. Cryst.* **1980**, *71*, 189.
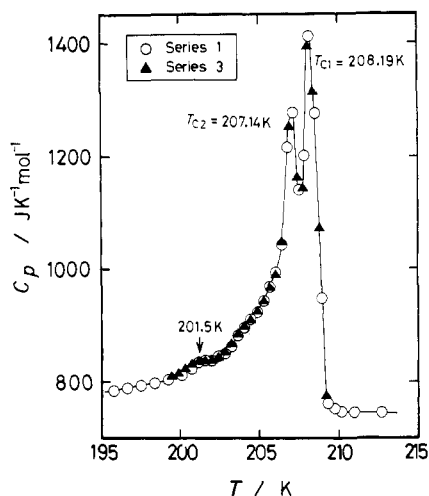
Figure 4. Molar heat capacity of [Fe₃O(O₂CCH₃)₆(py)₃](CHCl₃) in the vicinity of the phase transition region.

Calorimetric measurements were made in three series: series 1 (the temperature range from 80 to 302 K); series 2 (13–91 K); series 3 (199–261 K). The results were evaluated in terms of C_p, the molar heat capacity at constant pressure. The experimental data are listed in Table I and plotted in Figure 3. The two dominant thermal anomalies found by DTA were clearly observed by the heat capacity measurements as anomalies at 207.14 and 208.19 K. The temperatures of these transition points will be henceforth designated as T_{C_2} and T_{C_1}, respectively. Since the transitions occur in a narrow temperature interval, the heat capacities in this region are plotted in Figure 4 with an expanded scale of temperature. The nature of the two C_p peaks seen at T_{C_2} and T_{C_1} is discussed below. Heat capacity measurements in the phase transition region were made twice in series 1 and 3. Reproducibility was quite good between the two series. Thermal relaxation time, the time required for thermal equilibrium in the specimen after an electric energy input to the calorimeter cell, was shorter than 15 min in the normal temperature region where there is no effect of the phase transitions, while it was elongated to ~30 min or longer near T_{C_2} and T_{C_1}.

Thermodynamic Quantities Associated with Phase Transitions

To determine the excess heat capacities due to the phase transitions from the experimental C_p values, it is necessary to estimate a "normal" heat capacity curve. To this end, an effective frequency-distribution method[20] was employed. Since IR and/or Raman spectra are necessary for this method, IR spectra of [Fe₃O(O₂CCH₃)₆(py)₃](CHCl₃) were recorded in the range 4000–30 cm⁻¹ as a function of temperature. As described previously,[6] IR spectra of a given mixed-valence complex do not exhibit appreciable temperature dependence even if the electron localization–delocalization transformation occurs. This fact implies that the normal heat capacity might be represented by a single smooth curve without any discontinuity at the phase-transition points. The effective frequency-distribution method[20] assumes that the normal heat capacity of a solid arises from both a continuous phonon distribution and a number of discrete intramolecular vibrational modes. A borderline between them can be regarded as being 700 cm⁻¹ for the usual metal complexes such as the present compound. Since the present complex consists of 84 atoms, the number of degrees of freedom for a formula unit is 252. Among them, 38 modes of intramolecular vibration above 700 cm⁻¹ (143 degrees of freedom) were reasonably assigned on the basis of the IR spectrum with reference to the assignments for the related substances.[21,22] The contribution of these modes to the normal heat capacity was calculated according to the
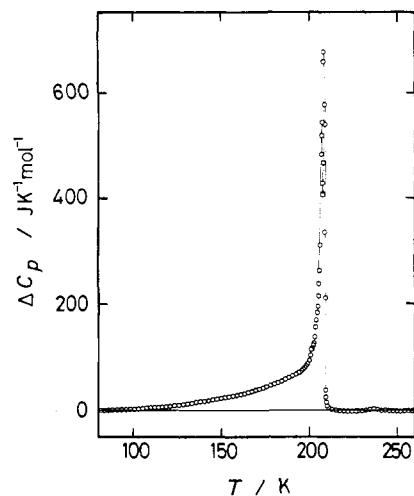
(20) Sorai, M.; Seki, S. *J. Phys. Soc. Jpn.* **1972**, *32*, 382.
(21) Corrsin, L.; Fax, B. J.; Lord, R. C. *J. Chem. Phys.* **1953**, *21*, 1170.
(22) Johnson, M. K.; Powell, D. B.; Cannon, R. D. *Spectrochim. Acta* **1981**, *37A*, 995.

Figure 5. Excess heat capacity, ΔC_p, due to the phase transition of [Fe₃O(O₂CCH₃)₆(py)₃](CHCl₃).
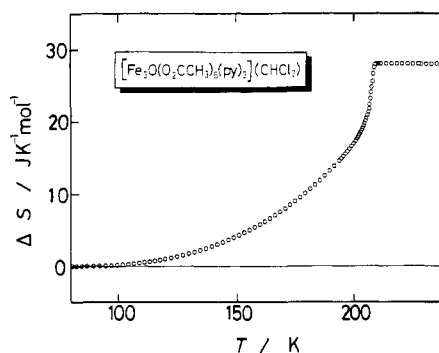

Figure 6. Acquisition of the transition entropy as a function of temperature for [Fe₃O(O₂CCH₃)₆(py)₃](CHCl₃) on the basis of the frequency spectrum E.

Einstein model. The contribution from the remaining 109 degrees of freedom was included in a continuous spectrum covering from 0 to 700 cm⁻¹, which consists of two Debye-type and three constant distributions. The contribution arising from the $(C_p - C_v)$ expansion work, where C_v is the heat capacity at constant volume, was effectively included in the continuous spectrum as if it would be equivalent to the contribution from some excess degrees of freedom.

The C_p versus T plot shown in Figure 3 definitely indicates that the thermal anomaly occurs from a temperature of ~100 K. For determination of the normal heat capacity, therefore, the temperature regions below 100 K and above 200 K were regarded as being normal, in which the effect of the phase transitions are negligible. By the use of 46 C_p values in the ranges 30–100 and 220–270 K, in which 10 C_p values around the small anomaly at 237 K were omitted, the "best" six effective frequency distributions below 700 cm⁻¹ were determined by the least-squares method. Combination of each continuous spectrum below 700 cm⁻¹ thus obtained and the discrete spectrum above 700 cm⁻¹ forms a complete set of an effective frequency distribution, and each set gives a normal heat capacity curve. The six sets of spectra are labeled A–F, respectively.

As shown in Table II, the present method reproduced the 46 experimental C_p values within a root-mean-squares deviation of ±(0.85–0.98) J K⁻¹ mol⁻¹, corresponding to ±0.1% of the observed C_p values. The total degrees of freedom characteristic of the frequency-distribution spectra from A to F were all about 262, which is by ~10 larger than the theoretical value of 252. The excess freedom is mainly due to the $(C_p - C_v)$ expansion work. A broken curve shown in Figure 3 corresponds to the normal heat capacity due to the frequency-distribution spectrum E, which we shall use as the representative normal heat capacity curve.

The difference between the observed and normal heat capacities is the excess heat capacity, ΔC_p, due to the phase transitions. In

Table I. Molar Heat Capacity of the Mixed-Valence Complex [Fe₃O(O₂CCH₃)₆(py)₃](CHCl₃)[a]

T, K	C_p, J K⁻¹ mol⁻¹	T, K	C_p, J K⁻¹ mol⁻¹	T, K	C_p, J K⁻¹ mol⁻¹	T, K	C_p, J K⁻¹ mol⁻¹
				Series 1			
81.570	420.64	154.340	646.10	201.994	837.96	228.752	776.66
83.599	428.07	156.565	652.52	202.410	845.51	231.011	781.84
85.795	436.48	158.774	658.93	202.827	850.33	233.261	787.46
88.205	445.49	160.968	665.07	203.240	862.71	235.501	793.11
90.823	455.03	163.146	671.64	203.650	881.91	237.732	798.92
93.382	464.13	165.311	678.31	204.057	896.06	239.955	802.33
95.886	472.24	167.461	684.87	204.464	910.46	242.172	805.82
98.342	480.32	169.598	691.74	204.870	922.79	244.382	809.74
100.753	488.06	171.722	698.25	205.267	942.86	246.584	813.08
103.124	496.04	173.853	704.82	205.661	967.06	248.781	817.42
105.456	503.73	175.991	712.15	206.049	992.72	250.969	822.15
107.755	511.22	178.116	718.87	206.432	1041.39	253.151	826.88
110.020	518.24	180.229	725.81	206.796	1216.29	255.325	830.71
112.256	524.86	182.330	732.88	207.142	1277.43	257.490	836.48
114.464	530.69	184.419	740.23	207.494	1140.51	259.825	842.36
116.645	537.01	186.495	747.99	207.851	1202.04	262.325	848.27
118.802	543.24	188.560	755.44	208.189	1411.30	264.814	853.86
121.146	550.25	190.613	763.20	208.522	1276.71	267.295	859.41
123.675	557.96	192.654	770.57	208.890	947.73	269.765	864.57
126.174	565.13	194.104	776.55	209.302	762.61	272.226	871.06
128.645	572.37	194.970	779.15	209.733	753.45	274.678	876.73
131.090	579.41	195.833	784.03	210.166	747.98	277.123	881.49
133.510	586.52	196.693	788.68	210.962	746.51	279.560	886.91
135.906	593.75	197.551	793.08	212.702	746.36	282.446	892.44
138.279	600.43	198.406	798.11	215.019	749.59	285.459	898.96
140.631	606.82	199.258	803.91	217.329	753.45	288.456	905.47
142.963	613.52	200.107	811.91	219.631	757.90	291.435	912.86
145.274	620.12	200.740	823.02	221.924	762.26	294.401	918.80
147.567	626.81	201.158	834.74	224.208	766.77	297.360	925.00
149.842	633.35	201.576	838.25	226.484	771.50	300.309	932.03
152.100	639.92						
				Series 2			
14.083	47.48	28.361	138.54	48.199	261.80	71.861	380.51
14.921	52.86	29.795	148.27	50.044	272.08	73.914	389.57
15.805	57.66	31.296	158.03	52.106	284.27	75.911	397.83
16.715	63.00	32.876	168.40	54.351	296.46	77.857	405.63
17.803	69.94	34.633	179.78	56.619	308.57	79.757	413.36
19.037	77.71	36.549	192.20	58.901	320.22	81.616	420.33
20.322	85.89	38.518	204.77	61.205	331.74	83.437	427.57
21.639	94.16	40.874	219.02	63.406	342.19	85.224	434.05
22.932	102.91	42.738	230.08	65.520	352.14	86.978	440.94
24.267	111.75	44.585	241.35	67.613	361.70	88.703	447.38
25.643	120.78	46.420	251.51	69.745	371.14	90.400	453.43
27.004	129.61						
				Series 3			
199.477	809.60	204.061	898.26	208.426	1313.64	245.500	812.39
199.902	814.55	204.465	909.06	208.782	1071.24	247.700	816.39
200.324	822.73	204.866	923.95	209.183	775.66	249.893	820.48
200.745	830.98	205.263	942.16	227.623	774.52	252.079	824.78
201.164	836.71	205.657	965.53	229.889	779.28	249.893	820.48
201.582	837.20	206.046	987.92	232.145	785.51	252.079	824.78
202.000	837.78	206.429	1045.47	234.391	791.59	254.258	829.91
202.418	843.03	206.914	1252.21	236.628	797.37	256.430	834.66
202.833	852.50	207.389	1162.10	238.857	800.89	258.596	839.33
203.246	866.87	207.749	1142.89	241.078	803.46	260.988	845.33
203.655	884.58	208.094	1393.23	243.293	808.81		

[a] Relative molecular mass = 894.490.

Figure 5, ΔC_p is plotted as a function of temperature. The enthalpy (ΔH) and entropy (ΔS) arising from the phase transition were determined by integration of ΔC_p with respect to T and ln T, respectively. The values of ΔH and ΔS estimated by using six different normal heat capacity curves are listed in Table II. The average values are $\Delta H = 5107 \pm 44$ J mol⁻¹ and $\Delta S = 28.10 \pm 0.44$ J K⁻¹ mol⁻¹. Figure 6 illustrates the acquisition of the transition entropy as a function of temperature based on the frequency spectrum E.

Nature of the Phase Transition

As can be seen in Figure 5, the phase transition found for [Fe₃O(O₂CCH₃)₆(py)₃](CHCl₃) exerts its effect down to ~100 K. The ΔC_p becomes gradually larger with increasing sample temperature above ~100 K. With further increase of the temperature the ΔC_p exhibits sharp double peaks centered at 207.14 and 208.19 K. Finally, at higher temperatures, ΔC_p suddenly decreases without showing any appreciable thermal anomaly due to short-range ordering. As judged from the temperature dependence of ΔC_p, the phase transition seems to consist of a combination of a higher order nature dominant at low temperatures and a first-order nature in the vicinity of the double peaks.

Transition entropy plays a diagnostic role in the elucidation of the nature of a phase transition. In particular, it provides us with a knowledge of how many molecular degrees of freedom are gained in a phase transition. The transition entropy determined for the present mixed-valence complex [Fe₃O(O₂CCH₃)₆-(py)₃](CHCl₃) (1) is $\Delta S = 28.10 \pm 0.44$ J K⁻¹ mol⁻¹. This value

Table II. Transition Enthalpy and Entropy of the Mixed-Valence Complex [Fe$_3$O(O$_2$CCH$_3$)$_6$(py)$_3$](CHCl$_3$)

spectrum	tot. deg of freedom[a]	$\sigma(E_p)$[b]	ΔH, J mol^{-1}	ΔS, J K^{-1} mol^{-1}
A	261.8	0.853	5108	27.94
B	261.4	0.983	5056	27.53
C	261.5	0.977	5075	28.76
D	261.7	0.937	5095	27.87
E	262.0	0.909	5128	28.09
F	262.4	0.852	5182	28.43

av 5107 ± 44

av 28.10 ± 0.44

[a] Theoretical value is 252 as [Fe$_3$O(O$_2$CCH$_3$)$_6$(py)$_3$](CHCl$_3$) consists of 84 atoms. The excess freedom is mainly due to the ($C_p - C_v$) expansion work. [b] Root-mean-squares deviation of the 46 C_p values from the calculated normal heat capacity curve.

is small in comparison with the ΔS value of 30.58 ± 0.83 J K^{-1} mol^{-1} observed for [Fe$_3$O(O$_2$CCH$_3$)$_6$(py)$_3$](py)[4,6] (**2**) and 35.8 J K^{-1} mol^{-1} observed for [Mn$_3$O(O$_2$CCH$_3$)$_6$(py)$_3$](py)[23] (**3**), whereas it is much larger than the 13.71 ± 0.65 J K^{-1} mol^{-1} value for [Fe$_3$O(O$_2$CCH$_3$)$_6$(3-Me-py)$_3$](3-Me-py)[11] (**4**), where 3-Me-py is 3-methylpyridine, and the 15.07 J K^{-1} mol^{-1} value for [Fe$_3$O-(O$_2$CCH$_3$)$_6$(3-Me-py)$_3$](toluene)[24] (**5**).

In the cases of complexes **4** and **5**, X-ray structural analysis[10] shows that the 3-methylpyridine and toluene solvate molecules are disordered in two positions in the high-temperature valence-detrapped phase. When fast intramolecular electron transfer occurs among the three iron ions in these complexes, the expected transition entropy is the sum of $R \ln 2$ arising from the dynamic disorder of solvate molecules in two positions and $R \ln 3$ due to the Fe$_3$O complexes interconverting rapidly between three vibronic states. The experimental entropy gain values for complexes **4** and **5** agree well with $R \ln 6$ (=14.90 J K^{-1} mol^{-1}). On the other hand, in the case of complex **2** the observed ΔS (=30.58 ± 0.83 J K^{-1} mol^{-1}) is well interpreted as being close to $R \ln 36$ (=29.79 J K^{-1} mol^{-1}), which could be the sum of $R \ln 3$ due to the Fe$_3$O complexes gaining access to three vibronic states and $R \ln 12$ due to pyridine solvate molecules becoming dynamically disordered among 12 positions. In the case of complex **3**, the ΔS (=35.8 J K^{-1} mol^{-1}) is close to $R \ln 72$ (=35.56 J K^{-1} mol^{-1}), which could be taken as the sum of $R \ln 4$ due to the Mn$_3$O complexes interconverting between four vibronic states and $R \ln 18$ due to the pyridine solvate molecule gaining access to 18 positions.[23]

If the CHCl$_3$ solvate molecule in complex **1** is disordered equally in two positions, one with the C–H vector pointing up along the crystallographic C_3 axis and the other with the C–H vector pointing down along the C_3 axis, the total transition entropy gain for the phase transition would be either $R \ln 8$ (=17.29 J K^{-1} mol^{-1}) or $R \ln 6$, depending on whether or not the "fourth" coherently electron-delocalized vibronic state without any distortion from the equilateral triangle is realized for the Fe$_3$O complex. However, neither of these ΔS values can account for the observed ΔS = 28.10 ± 0.44 J K^{-1} mol^{-1}. This fact clearly indicates that more disordering of the CHCl$_3$ solvate molecules is involved in the phase transition of [Fe$_3$O(O$_2$CCH$_3$)$_6$(py)$_3$](CHCl$_3$).

Since the ΔS (=28.10 ± 0.44 J K^{-1} mol^{-1}) for the present complex [Fe$_3$O(O$_2$CCH$_3$)$_6$(py)$_3$](CHCl$_3$) is very close to $R \ln 32$ (=28.82 J K^{-1} mol^{-1}), it is clear that the number of the disordered positions for the chloroform solvate molecules in the lattice at high temperatures is less than that for the pyridine solvate molecules but more than those for the 3-methylpyridine and toluene solvate molecules. Close examination of the ^{2}H NMR spectra for oriented

samples of [Fe$_3$O(O$_2$CCH$_3$)$_6$(py)$_3$](CDCl$_3$)[13] suggests that if the CDCl$_3$ solvate molecule is dynamically jumping between only two positions in which the C–D vector was pointing up and down along the C_3 axis, this would not account for the quadrupole splitting observed in the valence-detrapped phase. The authors[13] concluded that additional motion of the solvate molecule is involved and proposed two possible models. In one model the C–D vector is positioned not along the C_3 axis, but is imagined as jumping between three equally probable positions, where in each position the C–D vector is directed at the two oxygen atoms in one acetate group of the Fe$_3$O complex near to the chloroform solvate. Since the [Fe$_3$O(O$_2$CCH$_3$)$_6$(py)$_3$] and the CDCl$_3$ solvate molecules are stacked in alternate sites of 32 symmetry along the C_3 axis, there would be three positions of the C–D vector down and three positions up. In this model, the angle α between the C_3 axis and the C–D vector was calculated[13] to be 21.2° with an entropy gain of $R \ln 6$. The second model involves the C–D vector jumping between four positions of equal probability. Three of these four positions are as described above where now the angle α is 24.7°. The fourth position would be one in which the C–D vector is along the C_3 axis ($\alpha = 0°$). Since the CDCl$_3$ solvate molecule sits on a 32 symmetry site, the number of total positions of the C–D vector in this second model is 8 and hence the entropy gain is $R \ln 8$.

The 298 K single-crystal X-ray results for [Fe$_3$O(O$_2$CCH$_3$)$_6$-(py)$_3$](CHCl$_3$)[13] have several indicators which suggest that the C–H vector of the CHCl$_3$ solvate molecule is not just sitting on the C_3 axis but is likely jumping to positions off the C_3 axis. Motion of the C–H vector off the C_3 axis is indicated by the following facts:

(1) The anisotropic thermal parameters for the three Cl atoms are severely elongated in a direction along the C_3 axis. These thermal parameters indicate a disorder is present and are consistent with either of the two models given above.

(2) The C⋯C distance resulting from the disorder of the chloroform C–H moiety about the C_2 axis is longer, not shorter, than would be expected for a static CHCl$_3$ case. This indicates some off-C_3-axis motion.

(3) The C–H⋯O(acetate) distances between the chloroform solvate molecule and the nearby Fe$_3$O complex are large and would permit the CHCl$_3$ solvate molecule to move around relatively easily.

When the phase transition involves the Fe$_3$O complex changing from being trapped in one vibronic state to interconverting rapidly between three vibronic states, in each of which the "extra" electron is trapped on one iron ion, the entropy gain associated with valence detrapping in the Fe$_3$O complexes is $R \ln 3$. If this is the case for the Fe$_3$O complexes, the first model described above for the motion of the CHCl$_3$ solvate leads to a total entropy change of $R \ln 18$ (=24.03 J K^{-1} mol^{-1}), while the second model for the motion of the CHCl$_3$ solvate gives $R \ln 24$ (=26.42 J K^{-1} mol^{-1}). On the other hand, if the Fe$_3$O complexes gain acess equally to the fourth vibronic state where they are electronically delocalized in addition to the three dynamically distorted vibronic states, the entropy gain becomes $R \ln 4$ for the Fe$_3$O complex constituent. In this case, the first and second models for motion of the solvate molecule give total entropy gains of $R \ln 24$ and $R \ln 32$ (=28.82 J K^{-1} mol^{-1}), respectively. The present calorimetric value of 28.10 ± 0.44 J K^{-1} mol^{-1} is most favorably compared with $R \ln 32$.

Therefore, together with [Mn$_3$O(O$_2$CCH$_3$)$_6$(py)$_3$](py),[23] the present mixed-valence complex [Fe$_3$O(O$_2$CCH$_3$)$_6$(py)$_3$](CHCl$_3$) is revealed to be a rare example in which the fourth vibronic state of the Fe$_3$O complex, which involves coherent electron delocalization, is realized in the valence-detrapped state. At present, the experimental evidence supporting the coexistence for a Fe$_3$O complex of molecules in the fourth static vibronic state, which is electronically delocalized, and molecules interconverting rapidly between the three distorted vibronic states to give a dynamically distorting Fe$_3$O core in the high-temperature phase has been deduced only from the magnitude of the transition entropy determined in the present calorimetric measurements. Single-crystal X-ray diffraction analysis cannot distinguish between the presence of the two different vibronic states. ^{57}Fe Mössbauer spectroscopy

(23) Heat capacity measurements for [Mn$_3$O(O$_2$CCH$_3$)$_6$(py)$_3$](py): Nakano, M.; Sorai, M.; Vincent, J. B.; Christou, G.; Hendrickson, D. N. Manuscript in preparation.

(24) Heat capacity measurements for [Fe$_3$O(O$_2$CCH$_3$)$_6$(3-Me-py)$_3$](toluene): Nishimori, A.; Nagano, Y.; Sorai, M.; Jang, H. G.; Hendrickson, D. N. Unpublished results.
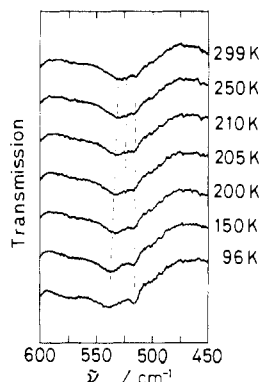
Figure 7. IR spectra of a Nujol mull of $[Fe_3O(O_2CCH_3)_6(py)_3](CHCl_3)$ in the range 600–450 cm^{-1} recorded at seven temperatures from 96 to 299 K.

also cannot distinguish them because the dynamic electron transfer is occurring at a rate greater than the Mössbauer time scale of $\sim 10^7$–10^8 s^{-1}.

No so definitive but important information is conceivably obtainable from an analysis of the characteristic IR band near 530 cm^{-1}, which has been assigned to the asymmetric stretch of the Fe_3O core, $\nu_{as}(Fe_3O)$.[25] This band is infrared active and is doubly degenerate when the planar Fe_3O core has D_{3h} symmetry, the case of the equilateral triangle that obtains for the fourth static electronically delocalized state. On the other hand, when the three iron ions in a given Fe_3O complex are not equivalent as in the other three distorted vibronic states, the degeneracy of this IR band is lifted to give a doublet in the IR spectrum. Since the rate of the intramolecular electron transfer is greater than the Mössbauer time scale ($\sim 10^7$–10^8 s^{-1}) but less than the IR time scale ($\sim 10^{14}$ s^{-1}), the temperature dependence of this band would be expected to provide us with useful information as to whether Fe_3O complexes frequent either of these two types of vibronic states. Figure 7 illustrates the IR spectrum of $[Fe_3O(O_2CCH_3)_6(py)_3](CHCl_3)$ in the 600–450-cm^{-1} range recorded at seven temperatures from 96 to 299 K. The spectrum recorded at 96 K, where it has been established that this complex is statically trapped in one of its distorted vibronic states, consists of a doublet at 540 and 515 cm^{-1}. With increasing temperature, this doublet gradually smears out. This smearing process seems to proceed with superimposing a single band at the center of the doublet. This new single band might arise from molecules in the static electronically delocalization vibronic state.

Although the mixed-valence complexes 1–3 crystallize in the identical rhombohedral space group $R32$ at room temperature, the phase transition behavior varies from one complex to another. Complex 2 exhibits two phase transitions; one is first order and occurs at low temperature (~ 112 K), and the other is higher order and culminates at higher temperature (~ 190 K). On the other hand, complexes 1 and 3 give essentially a single first-order phase transition. Kambara et al.[8] developed a theoretical model based on the molecular field approximation in order to show what types of phase transitions involving an electronic-delocalization transformation are possible in the trinuclear mixed-valence compounds and how the electronic structure of constituent Fe_3O molecules determines the type of phase transition. A phenomenological intermolecular interaction that depends on the sense and the magnitude of molecular distortion of a given Fe_3O complex arising from the electron localization was introduced in this model. Gross aspects of the phase transitions of complexes 1–3 are qualitatively explained by this model. However, this model does not seem to yield two phase transitions for such a Fe_3O complex.

Recently, an alternative theoretical model, which is basically similar to the Kambara et al. model[8] but can give two phase transitions, was proposed by Stratt and Adachi.[17] Since these two

(25) Dziobkowski, C. T.; Wrobleski, J. T.; Brown, D. B. *Inorg. Chem.* **1981**, *20*, 679.
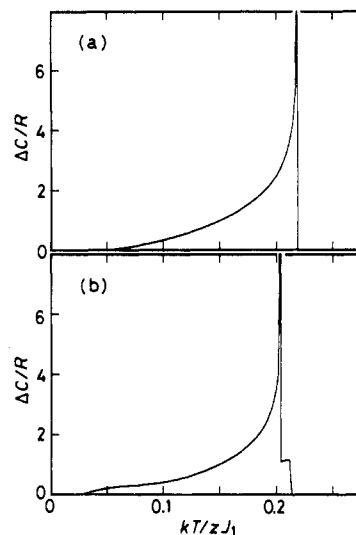

Figure 8. Excess heat capacities arising from the intramolecular electron transfer in a trinuclear mixed-valence complex calculated on the basis of the theory of Stratt and Adachi.[17] The ratio of interaction energy parameters J_2/J_1 for curves a and b are 0.6 and 0.8, respectively, and $J_3/J_1 = 0.25$ has been assumed for both calculations.

theoretical models have taken into account only the degrees of freedom concerning the distortion of the Fe_3O complex cores and have not treated the degrees of freedom arising from disordering of the solvate molecules, direct comparison of the transition entropies between the theory and experiment cannot be made. However, these theories give qualitative insights into the electron-delocalization mechanism.

According to the Hamiltonian given by Stratt and Adachi,[17] we calculated the excess heat capacity, ΔC, arising from the phase transition with two sets of intermolecular interaction parameters. The results are shown in Figure 8, in which R is the gas constant, k the Boltzmann constant, z the number of the nearest neighbors, and J_1 the interaction energy of two neighboring Fe_3O molecules, both of which are distorted parallel to each other. The two additional parameters necessary for characterizing the ΔC versus T curves shown in Figure 8a,b are J_2 and J_3. J_2 is the interaction energy of two neighboring molecules, only one of which is distorted. J_3 is the interaction energy of two neighboring molecules, both of which are distorted but at an angle of $2\pi/3$ with respect to each other. The adopted parameters are $J_2/J_1 = 0.6$ and $J_3/J_1 = 0.25$ for curve a, and $J_2/J_1 = 0.8$ and $J_3/J_1 = 0.25$ for curve b.

Curve a shows a single first-order phase transition between phases I and III (Stratt and Adachi's notation[17]). According to the author's definition, phase I corresponds to a significantly electron-localized phase where a preferred direction exists for the distortion of the localized metal complexes, while in phase III distorted and undistorted (electronically delocalized) complexes are randomly distributed and dynamically interconverting. Apart from the absolute value of ΔC, the theoretical curve a seems to reproduce the characteristic feature of the observed ΔC_p shown in Figure 5, in particular, a remarkable long tail of ΔC_p extending down to low temperatures.

Curve b was calculated to demonstrate how this theory[17] might give double peaks in the vicinity of the phase-transition point. With the parameters selected for curve b, the theoretical model predicts two phase transitions: one is a first-order phase transition between phases I and II, and the other is a second-order one occurring between phases II and III. According to the author's definition,[17] phase II consists of two sublattices, one containing mainly undistorted (delocalized) complexes and the other containing mainly distorted (localized) complexes, and no preferred direction for the distortion exists. Since the two C_p peaks observed at 207.14 and 208.19 K seem to arise from two first-order phase transitions, either the Stratt and Adachi model cannot be applied to the present mixed-valence compound or the presence of the two C_p peaks reflects the fact that the heat capacity sample was prepared in

three batches. We have concluded that the origin of the two C_p peaks for [Fe$_3$O(O$_2$CCH$_3$)$_6$(py)$_3$](CHCl$_3$) is *not* attributable to multiple batches in the sample preparation. Very recently we found that a large sample of isostructural [Fe$_3$O(O$_2$CCH$_3$)$_6$(4-Me-py)$_3$](CHCl$_3$) prepared in a single batch also exhibits two nearby first-order phase transitions, this time at 93.48 and 95.04 K. The presence of two nearby first-order phase transitions is an intrinsic feature of these two CHCl$_3$ solvates, a feature that is not explicable in terms of the Stratt and Adachi theory. It may be that the CHCl$_3$ solvate molecules first cooperatively experience an onset of dynamics followed immediately by a first-order phase transition involving a cooperative valence detrapping of the Fe$_3$O complexes.

As has been recently shown,[3-11] dynamics in a solid-state lattice affects dramatically the rate of intramolecular electron-transfer in a mixed-valence complex. For the present complex [Fe$_3$O-(O$_2$CCH$_3$)$_6$(py)$_3$](CHCl$_3$), we found that a drastic change in the rate of intramolecular electron transfer occurs as the result of a minor modification of the ligand and/or solvate molecule. ^{57}Fe Mössbauer spectra of the mixed-valence complex [Fe$_3$O-(O$_2$CCH$_3$)$_6$(4-Me-py)$_3$](CHCl$_3$), in which only the pyridine ligand of the present complex is replaced by 4-methylpyridine, show a change from a valence-trapped to a valence-detrapped pattern around 95 K. As shown in Figure 2b, the DTA thermogram of this complex shows a phase transition at 93–95 K, which is ~115 deg lower in temperature than the transition temperature of the complex with unsubstituted pyridine ligands. A plausible reason why the transition temperature of the complex with the 4-methylpyridine ligand is so much lower in comparison with the complex with unsubstituted pyridine seems to be as follows. Since the crystal structure of [Fe$_3$O(O$_2$CCH$_3$)$_6$(4-Me-py)$_3$](CHCl$_3$)[13] is identical with that of [Fe$_3$O(O$_2$CCH$_3$)$_6$(py)$_3$](CHCl$_3$), intermolecular interactions between neighboring Fe$_3$O complexes sitting on different stacking columns could be weakened by introducing three methyl groups along three radical directions of a Fe$_3$O core, whereas the intermolecular interaction within the same column would remain unchanged. The addition of the methyl substituents reduces the interstack intermolecular interaction because this is due to an overlapping of pyridine ligands between Fe$_3$O complexes. Thus, it would require less thermal energy to overcome the interstack intermolecular interactions, and the phase transition occurs at lower temperature in the 4-Me-py complex than in the py complex.

On the other hand, the mixed-valence complex [Fe$_3$O-(O$_2$CCH$_3$)$_6$(4-Me-py)$_3$](CH$_3$CCl$_3$), in which the CHCl$_3$ solvate molecule is replaced by bulky 1,1,1-trichloromethane, shows a phase transition at 125 K in a heating DTA thermogram (see Figure 2c). This phase transition arises from a valence detrapping as indicated by Mössbauer results.[13] The transition temperature is located between the 208 K value for [Fe$_3$O(O$_2$CCH$_3$)$_6$-(py)$_3$](CHCl$_3$) and the 95 K value for [Fe$_3$O(O$_2$CCH$_3$)$_6$(4-Me-py)$_3$](CHCl$_3$). Although introduction of bulky solvate molecules in the stacking column may elongate the distance between two Fe$_3$O cores in one stack, with the result that the intermolecular interaction between the two cores would be weakened, the transition temperature is higher than that of [Fe$_3$O(O$_2$CCH$_3$)$_6$(4-Me-py)$_3$](CHCl$_3$). This increase in transition temperature might be caused by the steric hindrance of the bulky CH$_3$CCl$_3$ solvate molecules in the lattice, for the intramolecular electron-transfer has been shown to be enhanced by strong coupling with the orientational disordering of the solvate molecules.

Concluding Comments

Heat capacity results for [Fe$_3$O(O$_2$CCH$_3$)$_6$(py)$_3$](CHCl$_3$) show that it exhibits two first-order phase transitions with C_p peaks at 207.14 and 208.19 K. The total entropy gain for both phase transitions was determined to be $\Delta S = 28.10 \pm 0.44$ J K^{-1} mol^{-1}. This experimental ΔS value is explicable in terms of two contributions, one ($\Delta S = R \ln 4$) for the Fe$_3$O complexes converting from being valence trapped in one vibronic state to dynamically interconverting between four vibronic states and the other ($\Delta S = R \ln 8$) from the CHCl$_3$ solvate molecules converting from being statically in one lattice position to being dynamically interconverting between eight lattice positions. The sum of these two terms, $\Delta S = R \ln 32$ (=28.82 J K^{-1} mol^{-1}), agrees with the experimental value.

There are two important implications that can be deduced from the heat capacity and physical characterization[13] of [Fe$_3$O-(O$_2$CCH$_3$)$_6$(py)$_3$](CHCl$_3$).

First, the ΔS value for the phase transition indicates that not only are the Fe$_3$O complexes gaining access to the three distorted vibronic states where the "extra" electron resides on one iron ion but also they are accessing the one undistorted electronically delocalized vibronic state in the middle of the "Mexican-hat" potential-energy surface.

Second, the ΔS value and results of the X-ray structure and solid-state ^{2}H NMR study indicate that the CHCl$_3$ solvate is becoming dynamic in this phase transition. Each CHCl$_3$ is sandwiched between two Fe$_3$O complexes and is disordered about a C_2 axis with its C–H vector basically either pointing up at one Fe$_3$O complex or down at the other Fe$_3$O complex. However, what is really intriguing is that the chloroform C–H vector appears to be tracking the changes in vibronic coordinates of the nearby Fe$_3$O complex. That is, the C–H vector pointing up into the cavity of a nearby Fe$_3$O complex is probably jumping between four positions, one with the C–H vector along the C_3 stacking axis and the other three where the C–H vector is pointing at pairs of acetate oxygen atoms of the three $^-$O$_2$CCH$_3$ moieties pointing down at the CHCl$_3$ solvate. The dynamic interconversion of Fe$_3$O complexes between their four vibronic states occurs cooperatively with the chloroform C–H vector moving between four positions. These processes are occurring cooperatively because the phase transition appears to have a predominance of first-order nature. It is difficult to know whether the changes in chloroform C–H vector directions occurs faster or slower than the rate of tunneling of the Fe$_3$O complexes between their four vibronic states. In fact, it is probably some cooperative lattice disturbance such as a soliton that leads to the cooperative motion of the Fe$_3$O and CHCl$_3$ moieties. If the C–H vector was static and directed at only one acetate group of a nearby Fe$_3$O complex, it is possible that the weak van der Waals interaction between CHCl$_3$ and the Fe$_3$O complex could affect the ground-state potential-energy surface of the Fe$_3$O complex and therefore affect the rate of tunneling of the Fe$_3$O complex. The two CHCl$_3$ solvate molecules sitting above and below a Fe$_3$O complex in the solid state are akin to a small portion of the solvent structure about a donor–acceptor redox pair in solution.